



# Movement of giant lipid vesicles induced by millimeter wave radiation change when they contain magnetic nanoparticles

Martina Albini<sup>1</sup> · Massimo Salvi<sup>2</sup> · Emiliano Altamura<sup>3</sup> · Simone Dinarelli<sup>4</sup> · Loreto Di Donato<sup>5</sup> · Andrea Lucibello<sup>6</sup> · Fabio Mavelli<sup>3</sup> · Filippo Molinari<sup>2</sup> · Umberto Morbiducci<sup>2</sup> · Alfonsina Ramundo-Orlando<sup>1</sup>

Published online: 10 September 2018  
© Controlled Release Society 2018

## Abstract

Superparamagnetic iron oxide nanoparticles are used in a rapidly expanding number of research and practical applications in biotechnology and biomedicine. Recent developments in iron oxide nanoparticle design and understanding of nanoparticle membrane interactions have led to applications in magnetically triggered, liposome delivery vehicles with controlled structure. Here we study the effect of external physical stimuli—such as millimeter wave radiation—on the induced movement of giant lipid vesicles in suspension containing or not containing iron oxide maghemite ( $\gamma\text{-Fe}_2\text{O}_3$ ) nanoparticles (MNPs). To increase our understanding of this phenomenon, we used a new microscope image-based analysis to reveal millimeter wave (MMW)-induced effects on the movement of the vesicles. We found that in the lipid vesicles not containing MNPs, an exposure to MMW induced collective reorientation of vesicle motion occurring at the onset of MMW switch “on.” Instead, no marked changes in the movements of lipid vesicles containing MNPs were observed at the onset of first MMW switch on, but, importantly, by examining the course followed; once the vesicles are already irradiated, a directional motion of vesicles was induced. The latter vesicles were characterized by a planar motion, absence of gravitational effects, and having trajectories spanning a range of deflection angles narrower than vesicles not containing MNPs. An explanation for this observed delayed response could be attributed to the possible interaction of MNPs with components of lipid membrane that, influencing, e.g., phospholipids density and membrane stiffening, ultimately leads to change vesicle movement.

**Keywords** Giant unilamellar vesicles · Magnetoliposomes · Millimeter waves · Vesicle motion · Image-based automatic analysis · Optical microscopy

---

Martina Albini and Massimo Salvi contributed equally to this work.

**Electronic supplementary material** The online version of this article (<https://doi.org/10.1007/s13346-018-0572-y>) contains supplementary material, which is available to authorized users.

✉ Alfonsina Ramundo-Orlando  
alfonsina.ramundoorlando@ift.cnr.it

- <sup>1</sup> Institute of Translational Pharmacology, CNR, Rome, Italy
- <sup>2</sup> Department of Mechanical and Aerospace Engineering, Politecnico di Torino, Turin, Italy
- <sup>3</sup> Department of Chemistry, University of Bari, Bari, Italy
- <sup>4</sup> Institute of Structural Matter, CNR, Rome, Italy
- <sup>5</sup> Department of Electrical, Electronics, and Computer Engineering, University of Catania, Catania, Italy
- <sup>6</sup> Institute of Microelectronics and Microsystems, CNR, Rome, Italy

## Introduction

The ability to provide doses of medicine inside the organism in a specific place and time over drug release from artificially designed drug carriers is one of the core challenges in biomedical research [1–4]. Numerous techniques have been proposed as possible ways to control the motion of biological and biocompatible nano- and microstructures, particularly lipid vesicles. Specially designed microfluidic devices can use differences in size, shape, and rigidity to physically separate particles. It is also possible to use light [5] and acoustic waves [6] to induce particle motion. Other approaches use self-propelling particles for delivering therapeutics, such as coagulation factors, small molecules, or other chemical or biological agents [7].

Of particular interest in the field of drug delivery is the use of externally controllable fields to direct the motion of drug

carriers. In this regard, magnetic resonance navigation approaches have been developed that, using magnetic nanoparticles embedded in microcarriers or microrobots, impart a directional propelling force by 3D magnetic gradients [8]. As far as the use of soft particles as drug carriers, electric fields have been demonstrated to induce large deformation in liposome vesicles both experimentally [9, 10] and theoretically [11, 12]. Electric fields can be used to sort cells and to induce the formation of pores in vesicle membranes. Magnetic fields also offer the opportunity to direct the motion of biologically compatible soft matter. Experiments have demonstrated that liposome vesicles tend to align with an externally applied magnetic field. This is due to the directional magnetic susceptibility difference of the lipids, which form the membrane of these vesicles [13]. Unlike electric and magnetic field effects, the influence of high-frequency electromagnetic fields on liposome vesicles has received much less attention.

Liposomes, as carrier systems, have been explored more than any other nano- and microparticles for various diseases ranging from cancer treatment to pain management [14] and occupy unique position in drug delivery technology. These systems have unique properties of flexibility in terms of size and composition, the easy modification of surface properties, and high biocompatibility, and they are able to incorporate drugs within both their aqueous core and their lipidic bilayers. Through such means, the pharmacokinetics of a drug can be controlled and dictated by the liposomal delivery system rather than the drug attributes [15]. The most common methods to favor drug leakage from liposomes are based on the destabilization of the system induced by an external stimulus, among them there is mild hyperthermia usually induced by micro-, radio-, or ultrasound waves [16, 17]. Thus, the knowledge of the behavior of liposomes in response to external physical stimuli such as millimeter waves would be very valuable for designing novel drug delivery systems.

The adequacy of liposomes as a carrier system for drugs strictly depends on their size; thus, liposomes with submicrometer diameter (i.e., large unilamellar vesicles) are commonly used for *in vivo* applications, while giant unilamellar vesicles (GUVs), with a diameter ranging between 1 and 100  $\mu\text{m}$  but with identical local arrangement of lipid bilayers, can be used as models to visualize with optical microscopic techniques the membrane perturbations occurring after the application of an external stimulus [18].

In our previous study [19], we used GUVs to directly observe their response to exposure to low intensity millimeter wave (MMW) at 53.37 GHz. This frequency is one of the frequencies—other than 42.22 and 61.2 GHz—officially used in non-invasive complementary medicine against a variety of diseases [20–22]. Real-time imaging observations by light microscopy showed three distinct effects: (1) on vesicles geometry, i.e., elongation consisting of an increase in their lengths and changes in their direction angle, (2) induced

diffusion of fluorescent dye di-8-ANEPPS located in the region between the aqueous phase and the hydrocarbon interior of the lipid bilayer, and (3) change in the direction of vesicle motion and relative attraction among them [19]. These effects were not dependent on increase in temperature; thus, they have been considered non-thermal effects [23].

To address the question of whether the abovementioned induced movement of vesicles is dependent on the action of MMW on lipid membrane, considered the main target for the interaction of MMW with biological systems [24], we have successively studied two different types of GUVs formed of neutral (egg-PC) and negatively charged phospholipids (egg-PC/PG) and introduced a specific quantization of trajectories taken by all vesicles before, during, and after MMW exposure [25]. A marked change in the direction of vesicle trajectories occurring at the MMW switch “on” has been observed. Furthermore, only in the case of charged GUVs preparation, the induced direction of vesicle trajectories was maintained also after the MMW switch “off” [25]. As an explanation of these results, we have proposed that the different behaviors between neutral and charged GUVs could be ascribed to the different distributions of the charge (1) internal to the vesicle membrane and (2) between the internal and external of the membrane.

The combination of liposomes and superparamagnetic iron oxide nanoparticles in hybrid structures represents a unique opportunity for achieving therapeutic objectives [26]. The liposomes can act to concentrate these small nanoparticles (i.e., lower than 15 nm) and shield them from the immune system. In turn, the iron oxide nanoparticles can be magnetically guided for targeting *in vivo* [27] and control drug release providing heating when exposed to external stimuli such as alternating current electromagnetic fields, typically micro- and radiowaves [28, 29].

The aim of this study is to add information on the ways to orient the motion of lipid vesicles containing iron oxide nanoparticles by evaluating changes induced on their direction of motion while applying MMW exposure. Vesicle trajectories were here analyzed using a new ad hoc microscope image processing strategy to determine the motion of vesicles subjected or not to MMW exposure. Furthermore, accurate characterization of MMW exposure conditions was carried out, following recommendation provided in literature [23, 30], for obtaining adequate interpretation and reproducibility of the result.

## Materials and methods

### Materials

L- $\alpha$ -Phosphatidylcholine (egg yolk PC), 6:0–18:1 1-palmitoyl-2-oleoyl-sn-glycero-3-phosphocholine (POPC), 16:0–18:1 1-palmitoyl-2-oleoyl-sn-glycero-3-phosphoglycerol (POPG), phosphate buffer, calcein, and mineral oil were purchased from

Sigma-Aldrich (St. Louis, MO). Organic solvents (spectroscopic grade) and pure distilled water were purchased from Carlo Erba Reagenti (Milano, Italy). Anhydrous, pro-analysis (p.a.) glucose, and sucrose (Fluka BioChemica, Switzerland) were used without further purification. Aqueous dispersion of  $10 \pm 2.5$  nm oleic acid-amphiphilic polymer-coated maghemite ( $\gamma$ - $\text{Fe}_2\text{O}_3$ ) nanoparticles was obtained from Ocean NanoTech (San Diego, CA).

### Preparation of GUVs containing or not containing MNPs

Giant unilamellar vesicles (GUVs) were prepared by the water droplet transfer method [31], with a slight modification as described elsewhere [32]. Briefly, an Eppendorf tube (1.5 ml) was filled with, and in, the following order: (1) the “outer” solution (0.5 ml, 5 mM sodium phosphate pH 7.4, 200 mM glucose); (2) interfacial phase (0.3 ml, 0.5 mM lipids (POPC/POPG 9/1) dispersed in mineral oil); and (3) a water/oil emulsion (0.6 ml) prepared by pipetting up and down the inner phase (20  $\mu\text{l}$ , 5 mM sodium phosphate (pH 7.4)–200 mM sucrose, containing maghemite ( $\gamma$ - $\text{Fe}_2\text{O}_3$ ) nanoparticles (MNPs) at a concentration of 3 nmol/ml, in POPC/POPG (0.5 mM) suspended in mineral oil). The tube was centrifuged two times: firstly at  $300\times g$  for 10 min and secondly at  $2500\times g$  for a further 10 min at room temperature with fresh outer solution to remove mineral oil and any non-entrapped MNPs. Giant unilamellar vesicles containing MNPs (i.e., the visible pellet on the bottom of the tube) were re-suspended in 100  $\mu\text{l}$  final volume of 5 mM sodium phosphate (pH 7.4)–200 mM glucose.

The same procedure was adopted to prepare GUVs not containing MNPs by not adding MNPs in the abovementioned inner phase.

To provide a positive control of vesicle motion, the same giant unilamellar vesicles used in previous studies [19, 25] were prepared from electrically neutral phosphatidylcholine (i.e., egg-PC) by using the electroformation method applied to lipid films spin-coated on 45 mm  $\times$  45 mm glass slide covered with indium tin oxide (ITO) as extensively described in [25].

All steps of vesicle preparations were performed at room temperature, which is above the main phase transition one of POPC/POPG mixture or egg-PC; thus, the vesicle membrane should be in the fluid-like state.

### Quantitative analysis of MNPs contained in GUVs

Quantitative analysis of internal MNP concentration in GUVs was conducted with colorimetric *o*-phenanthroline method assay of iron, by measuring the absorbance of Tris (1,10-phenanthroline) iron(II) complex at  $\lambda = 500$  nm [33]. Briefly, 100  $\mu\text{l}$  of the MNP-GUV suspension was diluted 1:10 in  $\text{HNO}_3$  (31.5%) and HCl (18.5%) and incubated on a

hotplate. After cooling, the mixture was dissolved in 22 ml of HCl (3.7%) and iron (III) was reduced with hydroxylamine to the ferrous state. After the addition of 1,10-phenanthroline (1.0 g/l), the pH was adjusted to 3.0–3.5 by adding HCl. Iron content was determined with  $[\text{Fe}^{2+}]$  from 0 to 5 mg/ml as standard.

### Qualitatively analysis of GUVs containing MNPs

To ascertain that, GUVs containing MNPs were morphological stable water-soluble fluorescent probe (i.e., calcein disodium salt) was used as fluorescent markers of the aqueous GUVs cavity. Calcein entrapment was determined and imaged by confocal laser scanning inverted microscope (LEICA SP5II) on fresh and aged MNP-GUV preparations (i.e., maintained 24 h at room temperature in the dark). Digital image processing and analysis was carried out using ImageJ software.

### Millimeter waves setup and exposure protocol

The exposure experiments were performed at low intensity millimeter wave with frequency of 53.37 GHz by using a conical horn antenna (IMG-53.37, Micro Med Tech, Russia) with 34 mm maximal diameter and an output power of 39 mW. The distance between the centre of the observation dish and the horn antenna was 8 cm, and the incidence angle was downward at  $45^\circ$  to the vertical (see Supporting Information Fig. SI-1). This position of antenna minimizes reflections from the bench returning through the sample; thus, it was mainly exposed to the incident wave, avoiding additional power absorption from the reflected wave, as described in literature [34].

The same exposure protocol previously used [19, 25] was as follows: a polystyrene exposure chamber made of four separate dishes that were devoided of any conductive materials was placed on the microscope stage (Fig. 1). Each dish was filled with 1.5 ml of 200 mM glucose solution covering  $\approx 8$  mm of the dish height (10 mm). The dishes were processed separately and carefully checked for level using a circular spirit level. A small amount of vesicles suspension (2–4  $\mu\text{l}$ ) was added just to the dish under study so that only a few vesicles were freely dispersed in the glucose solution in order to minimize vesicles interaction. In order to evaluate the effects of exposure, vesicles were selected one at a time following the criteria that they were not connected to others and did not have internal formations or visible protuberances, as suggested elsewhere [35].

GUVs—the exposed samples—were subjected to 53.37 GHz radiation, which was switched on and off intermittently at the time intervals indicated in the “Results and discussion” section. Other GUVs—the sham samples—were not subjected to this radiation.

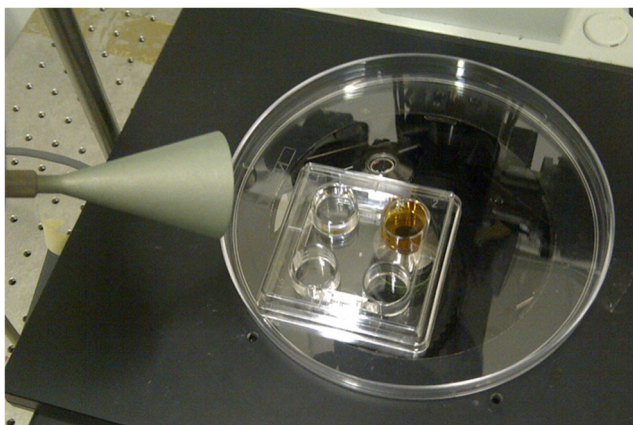


**Fig. 1** Exposure experiments were performed at low intensity millimeter wave with frequency of 53.37 GHz using a conical horn antenna (on the left). The exposure chamber (polystyrene four dishes) on the microscope stage is shown, where the dish under study has been colored in brown for visibility in this photograph

Accurate temperature measurements inside the samples were taken using a four-channel analog devices electronic thermocouple equipped with a flexible implantable probe (Physitemp Instruments, Inc., Type IT-18) of 0.06 cm diameter, 1 m lead length, 0.1 s time constant, and resolution of 0.01 °C. The probe tip of the thermocouple was placed in the central region of the aqueous solution containing GUVs, where microscope images were always collected.

### Optical microscopy analysis

To study the movement of vesicles, real-time imaging observations were carried out with an Olympus IX 70 inverted microscope (Rungis, France) in phase contrast mode, equipped with an optical condenser and a 20× objective lens with a total magnification of × 200. A high-speed camera having a 1-kHz frame acquisition rate (F-View II—Soft Imaging System GmbH, Germany) was used to record images. The best optical contrast was obtained by using diffraction index asymmetry of the solutions 200 mM sucrose inside and glucose outside the vesicles, as extensively described elsewhere [25]. The best focal planes were in the central region of the observation dish, corresponding to ≈ 3–4 mm of its height, where it was possible to observe the vesicles over the entire time of experiment before they approached the bottom of the dish. Further, at the start of the experiments, the area of observation was fixed and the focus plane and microscope light intensity were adjusted to obtain the highest definition of the edge of the selected vesicle, which is not necessarily coincident with the best optical contrast between inner and outer vesicle solution—usually obtained only when vesicles are stabilized by gravity at the bottom of the observation dish as indicated elsewhere [36]. Then, sequences of up to 20 images of the fixed area of observation were taken and recorded every minute. The microscope light was switch on only for the short

time needed for the image’s capture. Particular attention was given to avoiding any possible artifacts influencing the motion of vesicles. To maintain the stability of the test bench, the microscope was placed onto a Newport air-controlled anti-vibration table; the turning on/off of the microscope light, camera, and MMW antenna was governed by a single push button placed on a separate table.

### Vesicle motion analysis

A fully automated strategy was applied to process the microscope images of vesicles. Technically, a two-step algorithm was implemented for the automatic detection of all vesicles in each image frame and for the reconstruction of selected GUVs. The algorithm was developed within the Matlab™ (MathWorks, Natick, MA, USA) environment. The first processing step automatically detected the position of vesicles within each image frame (Fig. 2a). This task was achieved by applying the Hough transform [37], which permitted the identification of all the circular objects inside each single frame (Fig. 2b) and the subsequent deletion of concentric/intersecting objects (Fig. 2c). The second processing step was devoted to the reconstruction of the trajectory described by each identified vesicle during its motion. The trajectory of each vesicle in a sequence of image frames (Fig. 2d) was plotted, commencing with the largest, as follows: identify the position of the vesicle with the most similar size within a distance equal to five times the vesicle’s radius, draw a connection between the two, and repeat for each pair of consecutive frames in the sequence.

The algorithm also evaluated the 2D trajectory deflection, in terms of the instantaneous angle between the vector connecting two consecutive points of the vesicle trajectory and a reference direction (which was set as the horizontal one, the same in all image frames, corresponding to the  $y$ -axis of the reference coordinate system adopted here). Finally, the algorithm combines the in-plane trajectory of each vesicle with its through-plane trajectory (as evaluated from GUV segmentation, performed over each image frame) for fully three-dimensional characterization of each GUV trajectory: By assuming that, a vesicle does not change in size during its recorded motion; then, apparent variations in its radius during the experiment can give a measure of its position along the camera axis relative to the in-focus plane.

## Results and discussion

### Characterization of GUVs containing MNPs

GUVs containing superparamagnetic iron oxide nanoparticles (MNPs) prepared by the “droplet transfer” method were spherical (Fig. 3). Chiba and co-workers previously showed



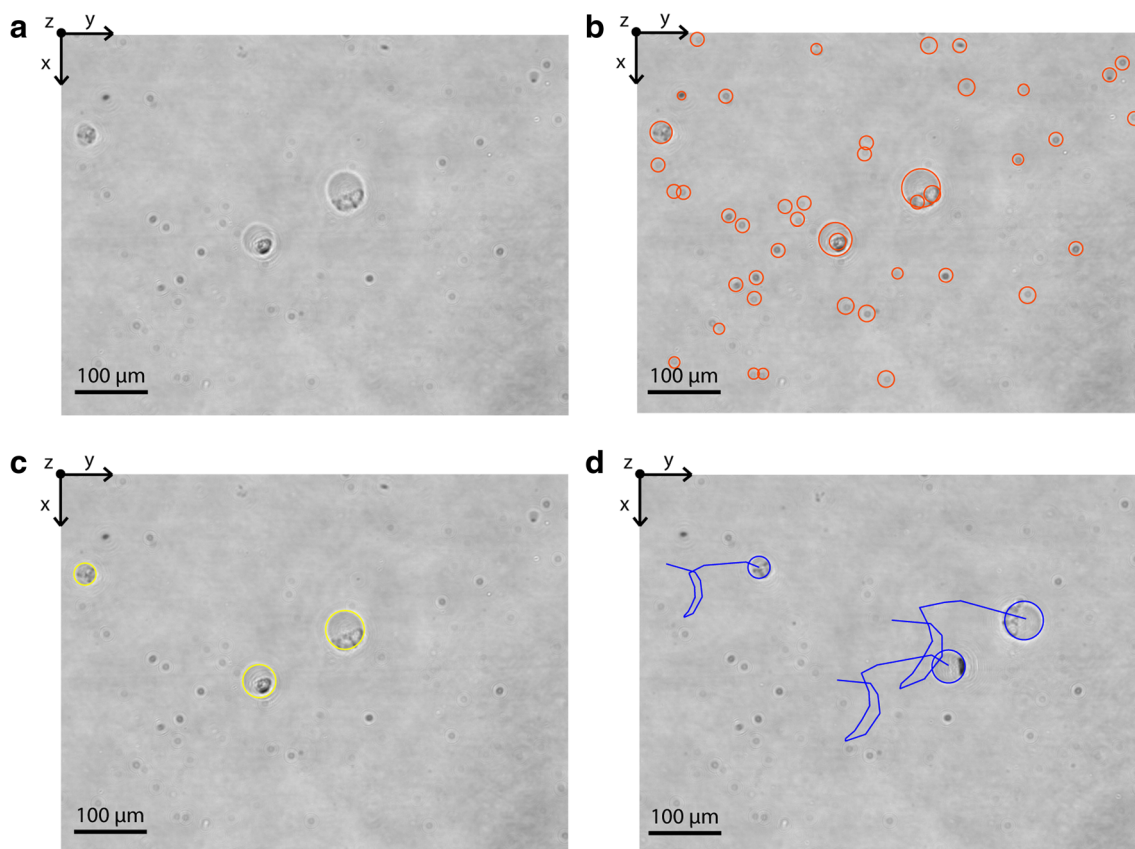


**Fig. 2** Image-based analysis. **a** Original image. **b** Circular object detection within the image using the Hough transforms. **c** Position of vesicles inside the frame after the deletion of concentric/intersecting

objects. **d** Reconstruction of the entire trajectory described by each vesicle during its motion. GUVs not containing MNPs (i.e., empty GUVs) are shown

that GUVs obtained through this droplet transfer method were unilamellar [38]. A prerequisite for successful investigation of the effects induced by MMW exposure is the morphological stability of vesicle preparations. In this context, no significant differences in the fluorescence intensity distribution of water-

soluble probe (i.e., calcein) were observed between the fresh and aged (i.e., 24 h) MNP-GUV preparations. Furthermore, the double washing by centrifugation carried out during the preparation of MNP-GUVs ensured that any MNPs not entrapped in the lumen of vesicles were removed.

Finally, the hydrophilic shell of MNPs and the dimension of nanoparticles (i.e., 10 nm) ensured that MNPs were loaded in GUVs lumen and not bound to the membrane surface or embedded into the bilayer [39]. The calculated internal amount of MNPs, determined by the absorbance of the iron(II) complex, was  $2.2 \pm 0.1 \mu\text{M}$ . For GUVs with a mean diameter of  $20 \mu\text{m}$ —used throughout this work—an average number of MNPs equal to  $5.4 \times 10^6$  per each GUVs preparation can be estimated, corresponding to a mass increase, for a single GUV, of  $1.2 \times 10^{-11} \text{ g}$ . This is similar to saying that a percentage mass increase of  $\approx 0.2\%$  was achieved after encapsulation of MNPs.

### Characterization of MNP-GUV motion

To provide an experimental control of vesicle motion, we analyzed the dynamics of GUVs containing MNPs in the absence of MMW exposure. A sample of these data, from six independent experiments, is shown in Fig. 4a, displaying two

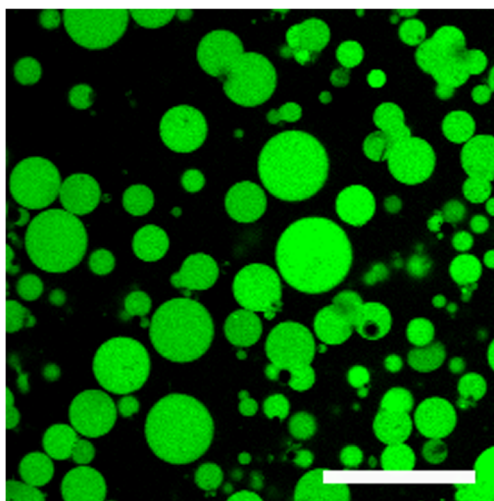


**Fig. 3** Formation of GUVs (POPC/POPG 9/1) containing internal concentration of MNPs ( $2.2 \pm 0.1 \mu\text{M}$ ) and calcein ( $10 \mu\text{M}$ ) are shown. Fluorescence confocal microscopy image is shown. Bar  $50 \mu\text{m}$

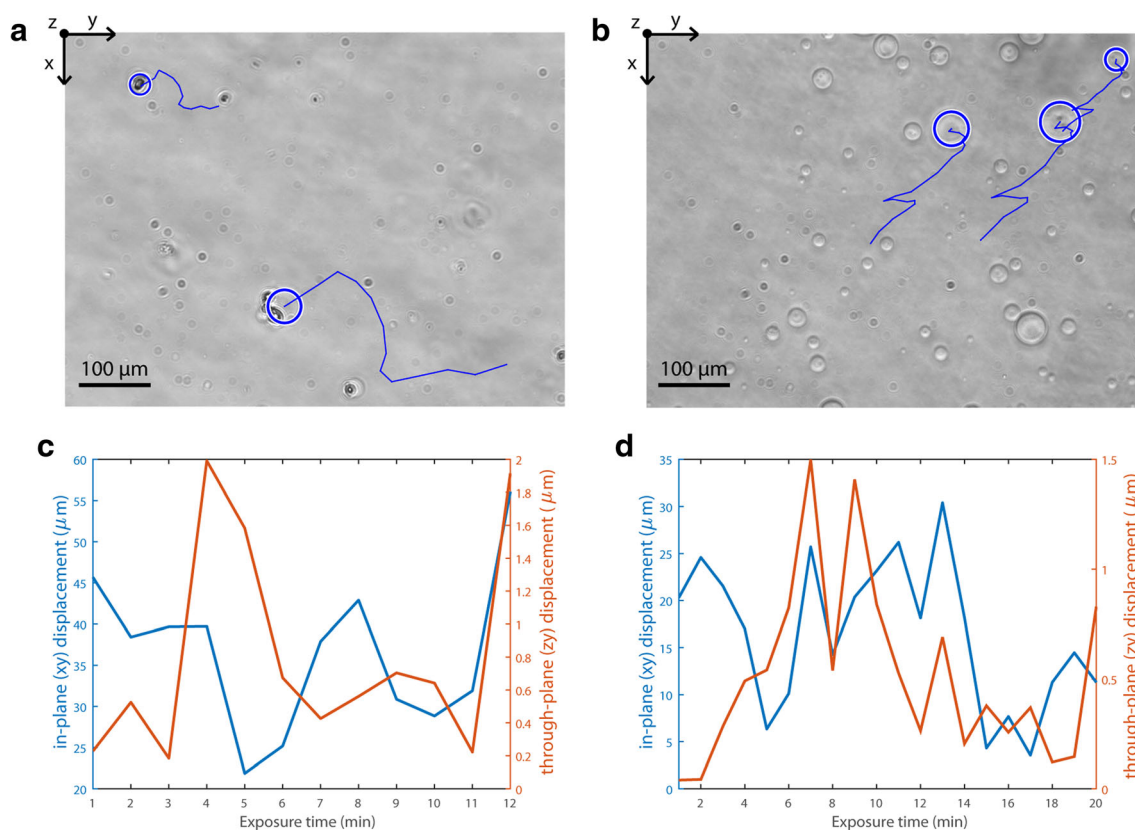


**Fig. 4** Vesicles dynamics under sham condition. **a** Image frame with the trajectory of two individual MNP-GUVs is shown. **b** Image frame with the trajectory of three individual neutral electroformed giant vesicles is

shown. **c** Comparison between in-plane ( $xy$ ) displacement and through plane ( $zy$ ) displacement for a vesicle in **a**. **d** Comparison between in-plane ( $xy$ ) displacement and through-plane ( $zy$ ) displacement for a vesicle in **b**

MNP-GUV trajectories overlaid. In this specific case, the sequence of 13 microscope images was analyzed for the trajectories related to two individual MNP-GUVs.

Since we previously used giant vesicles formed of egg-PC and prepared using a different method, such as electroformation, to study the dynamics of vesicles subjected to MMW exposure [19, 25], here, again, we used the same vesicle preparation as a positive control and to compare their dynamics with that of MNP-GUVs prepared using the droplet transfer method. Our aim was to show that the proposed experimental setup could allow the observation of vesicles dynamics independently from the type of phospholipids and/or preparation used. A sample of these data, from three independent experiments, is shown in Fig. 4b, displaying three neutral giant vesicle trajectories overlaid. In this specific case, the sequence of 21 microscope images was

analyzed for the trajectories related to three individual neutral giant vesicles. Hence, it is evident that in both cases, a collective motion is observed with non-preferential directions in lateral displacements. Furthermore, from the three-dimensional characterization of vesicle trajectories, accurately described in “Materials and methods,” in both cases, vesicle motion was mainly characterized by an in-plane ( $xy$ ) displacement of one to two orders of magnitude greater than through-plane ( $zy$ ) displacement (Fig. 4c, d). Similar results were also found for vesicle dynamics analysis of GUVs not containing MNPs (i.e., empty GUVs) (Table 1). It appears that phospholipid vesicles, generally, have high rates of lateral diffusion, as stated elsewhere [40], independently from the phospholipids composition and type of preparations. A similar random in-plane motion during image acquisition of vesicles by confocal fluorescence

**Table 1** Three-dimensional characterization of vesicles trajectory: in-plane and through-plane displacement (mean  $\pm$  standard error of the mean) for all analyzed vesicles in different samples subjected to MMW exposure

Type of vesicle	No. of sample	Displacement	
		In-plane ( $\mu\text{m}$ )	Through-plane ( $\mu\text{m}$ )
Neutral giant vesicles	3	$81.19 \pm 5.76$	$0.76 \pm 0.12$
Empty GUVs	3	$34.14 \pm 4.71$	$0.79 \pm 0.10$
MNP-GUVs	6	$37.41 \pm 2.31$	$1.33 \pm 0.11$

microscopy was also reported [41]. Furthermore, a similar behavior was also reported in a study of sedimentation process of vesicles in isotonic conditions, which presented significant lateral displacements [42]. Hence, in the absence of MMW exposure, vesicle motion is mostly planar, with gravity (vertical motion) playing a negligible role during the observation time. That is to say that under our carefully controlled experimental conditions, the observed vesicle motion could only be minimally ascribed to a sedimentation process of vesicles.

### MMW induces a change of MNP-GUV motion

The image-based analysis allowed us to identify trajectories taken by all vesicles before, during, and after MMW exposure. In a first attempt, the visual inspection of sequence of microscope images acquired during vesicle dynamics observation revealed that all vesicles were characterized by similar trajectories independently from their dimensions (see in Supporting Information Fig. SI-2). As a consequence, the vesicle selected for the image-based analysis of the dynamics could be considered, in any case, statistical representative of all many vesicles present in the observation dish. Vesicle movement was analyzed on microscope images of MNP-GUVs subjected to

MMW exposure intermittently switched on and off at 5-min intervals for a total time of 20 min. A sample of these data, from six independent experiments, is shown in Fig. 5a, displaying the entire trajectory of one MNP-GUV color-coded under sham (blue) and exposure (red) conditions. In this specific case, the sequence of 21 microscope images was analyzed for the trajectories related to one vesicle. A markedly in-plane motion for the MNP-GUV is observed (Fig. 5b) before, during, and after MMW exposure. We analyzed the vectors taken by the vesicle in the dataset (Fig. 5c), finding that the trajectory was highly polarized with a preferential displacement, independent from the exposure condition, where the vector components runs parallel to the  $y$ -axis in the negative direction, which in our coordinate system is to the left and is the same side as the MMW antenna (indicated by the arrow in Fig. 5c). Furthermore, no marked change in the vesicle direction at the onset of MMW-switch on ( $SHAM_1$  vs.  $IRR_1$ ; Fig. 5c) was observed. But, importantly, by examining the course followed once the vesicle was already irradiated, we found a clear trajectory deflection when the MMW exposure was switched off ( $IRR_1$  vs.  $SHAM_2$ ; Fig. 5c), with realignment in the direction previously taken at the first MMW switch on ( $IRR_1$  vs.  $IRR_2$ ; Fig. 5c). This finding leads us to conjecture

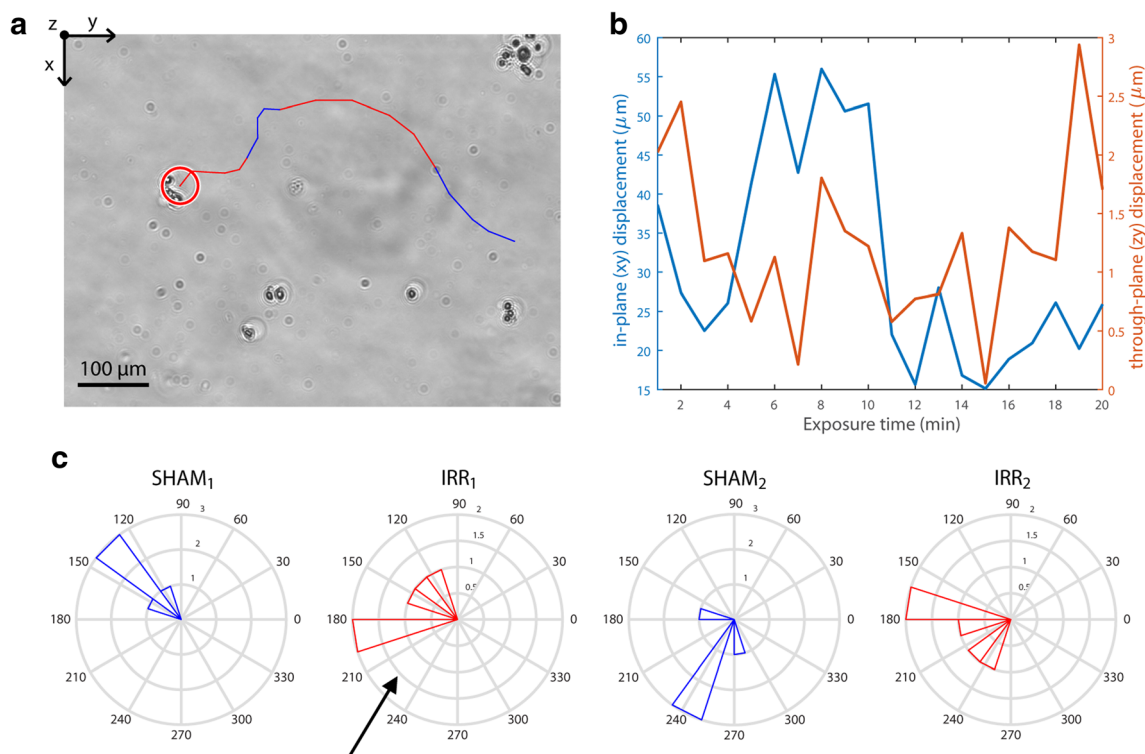


**Fig. 5** MMW changes MNP-GUV motion. **a** Image frame with the entire trajectory of one MNP-GUV color-coded under sham (blue) and exposure (red) conditions. **b** Comparison between in-plane ( $xy$ ) displacement and through-plane ( $zy$ ) displacement for the vesicle. **c** Rose diagrams are angular histograms of the distribution of instantaneous angular values showing the direction of vesicle motion in

terms of relative frequency. A direction of  $0^\circ$  indicates  $+y$  motion where vector component runs parallel to the positive  $y$ -axis pointing to the right. A direction of  $180^\circ$  indicates  $-y$  motion  $180^\circ$  where vector component runs parallel to the negative  $y$ -axis pointing to the left. Arrow depicts the side position of MMW antenna (color figure online)

that during MMW exposure, a directional motion of MNP-GUVs can be induced.

### MMW induces a change of empty GUV motion

We previously compared neutral (i.e., egg-PC) and negatively charged (i.e., PC/PG) giant vesicles prepared using the electroformation method [25] to relate the MMW-induced change in the direction of vesicle motion with the presence of charge and dipolar molecules at the bilayer/water interface region of the lipid bilayer [43]. This correlation was confirmed as MMW-induced change on the direction of vesicle motion was observed to a larger extent on giant vesicles prepared with negatively charged phospholipids than with neutral ones [25]. Here, accordingly, GUVs containing and not containing MNPs were both formed of negatively charged phospholipids (POPC/POPG); thus, by comparing them, it was possible to relate the MMW-induced change in the direction of vesicle motion only with the presence of MNPs in the lumen of former vesicles. To do this, the same experiments and analysis were performed on GUVs not containing MNPs (i.e., empty GUVs). A sample of these data, from three independent experiments, is shown in Fig. 6a, displaying the entire trajectory

of one empty GUV. In this specific case, the sequence of 20 microscope images was analyzed for the trajectories related to one vesicle. In agreement, a prevalent in-plane motion is also observed for empty GUV (Fig. 6c). Instead, the overall trajectory of empty GUV was characterized by the spread of vesicle deflection values larger than GUVs containing MNPs (Figs. 6c vs. 5c), indicating that the trajectory was not polarized. Furthermore, a marked change in the direction of vesicle motion occurs at the first MMW switch on ( $SHAM_1$  vs.  $IRR_1$ ; Fig. 6c) and at the first switch off ( $IRR_1$  vs.  $SHAM_2$ ; Fig. 6c). These results confirming previous observations on giant vesicles prepared using the electroformation method, where the switch on/off character of the MMW-induced effects was extensively described [19, 25], allowed a common explanation of the obtained results.

Under the proposed exposure condition, the energy content associated with electromagnetic fields has insufficient strength to modify the inherent structure of the region hit by the electromagnetic wave [44–46]. Thus, a different phenomenon can be proposed for explaining the obtained results: the interaction between the electromagnetic field and the charged structure can result, under given conditions, in a resonant (non-thermal) phenomenon which does not affect the structure

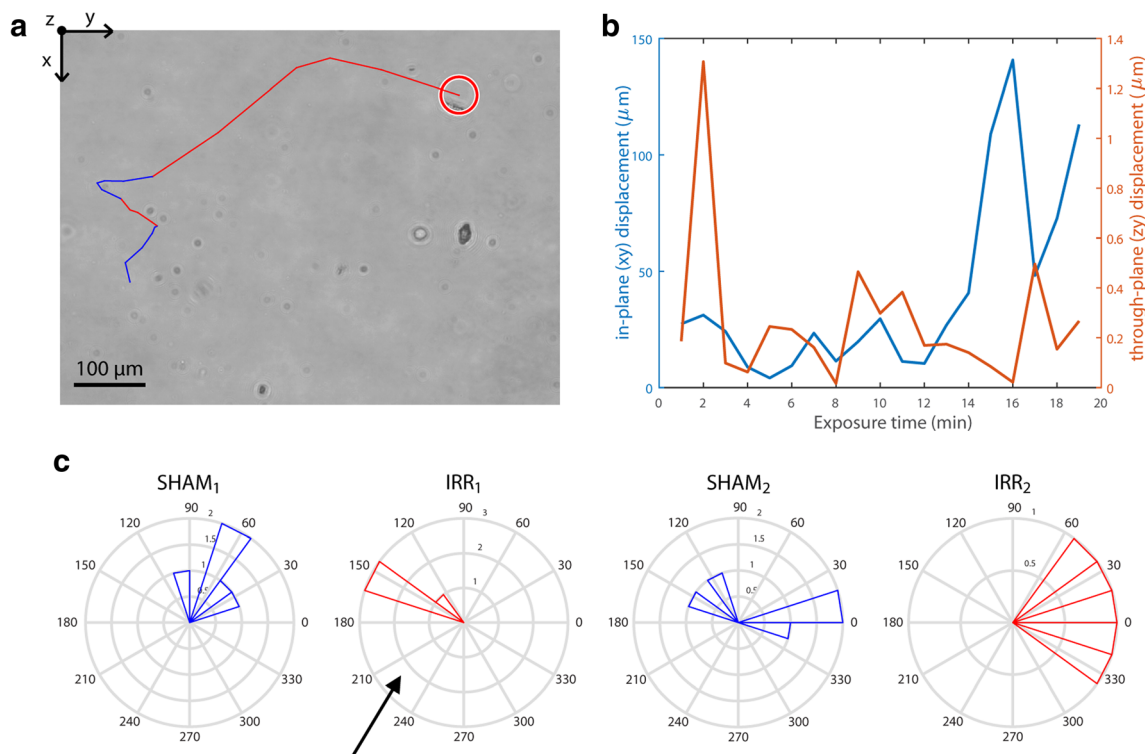


**Fig. 6** MMW changes empty GUV motion. **a** Image frame with the entire trajectory of one empty-GUV color-coded under sham (blue) and exposure (red) conditions. **b** Comparison between in-plane ( $xy$ ) displacement and through plane ( $zy$ ) displacement for the vesicle. **c** Rose diagrams are angular histograms of the distribution of instantaneous angular values showing the direction of vesicle motion in

terms of relative frequency. A direction of  $0^\circ$  indicates  $+y$  motion where vector component runs parallel to the positive  $y$ -axis pointing to the right. A direction of  $180^\circ$  indicates  $-y$  motion  $180^\circ$  where vector component runs parallel to the negative  $y$ -axis pointing to the left. Arrow depicts the side position of MMW antenna



from a thermal point of view but can induce mechanical modifications (e.g., motions) that could lead to biological changes.

By using a fast imaging digital camera, with a high temporal resolution (one image every 33  $\mu\text{s}$ ), observations of giant lipid vesicles subjected to electromagnetic field had shown a transient vesicle deformation [36], which the authors explained due to a reorganization of charges both internal and external to the membrane of vesicle [47, 48]. Although, the time scale of these phenomena is orders of magnitude smaller than the observation times of our study, and the image time resolution (one image every 50 ms) we used is not sufficient to detect small shape deformations, a similar transient deformation of the vesicles could result and contribute to the observed changes in direction of the vesicle motion when the MMW is switched on. However, it should be mentioned here, that there is still no evidence that, e.g., AC electric fields in the range of frequency of millimeter waves could lead to deformations in the shape of the vesicles [10].

In this scenario, the difference observed in the dynamics of GUVs containing MNPs vs. empty GUVs, i.e., GUVs containing MNPs do not markedly modify the direction of their motion at the onset of MMW switch on, could be ascribed to the interaction of MNPs with membrane components that could modify the vesicle transient deformation. In principle, the MNPs (i.e., hydrophilic uncharged particles of large size  $\approx 10$  nm) for inclusion limits between the bilayer would prefer to remain in the lumen of the GUVs rather than to be embedded into the lipid bilayer [49]. Nevertheless, MNPs could be shedding the oleic acid/polymer ligands, which, in turn, could embed into the membrane changing its dynamics, but, importantly, interaction of iron with the phosphate terminus of lipid head groups could be also possible. This latter interaction, by increasing the tilt angle, could enlarge the area of the head groups, as reported for giant vesicle of mixed DOPC/DOPG [50], thus leading to an enhancement of phospholipids density and subsequent membrane stiffening. Interestingly, the polar

head groups of the surface layer can affect the physical properties of the entire membrane as showed in a computer simulation study of dynamics of surface lipid membrane [51].

### Vesicles velocity under sham and exposure conditions

To investigate further the influence of MMW on vesicle dynamics, we also calculated the average in-plane velocity (expressed as  $\mu\text{m}/\text{min}$ ) of vesicles under study. Firstly, we analyzed the velocity of MNP-GUVs and empty GUVs and, for reference, of neutral giant vesicles prepared using the electroformation method in the absence of MMW. The analysis of these data, from three independent experiments, revealed no marked difference between the average in-plane velocity magnitude of MNP-GUVs and empty GUVs ( $36.58 \pm 1.73$  vs.  $33.06 \pm 2.43$   $\mu\text{m}/\text{min}$ ). This supported the small increment of mass between GUVs containing and not containing MNPs calculated to be less than 0.2%, thus indicating no influence of MNPs on the vesicles velocity. On the other hand, MNP-GUVs and empty GUVs exhibited an average in-plane velocity magnitude nearly double with respect to that of electroformed neutral giant vesicles ( $16.45 \pm 1.73$   $\mu\text{m}/\text{min}$ ).

We then analyzed the vesicles velocity on samples subjected to MMW exposure. This analysis revealed that in the case of electroformed neutral giant vesicles and empty GUVs, the average in-plane velocity increased by a factor around 4 during MMW exposure (Fig. 7a, b). Instead, lower increase in the average in-plane velocity magnitude of MNP-GUVs was observed (Fig. 7c). Representative samples of these data from MNP-GUVs and empty GUVs are shown in Fig. 8.

Together, these experiments show that the vesicle motion, mainly planar (in-plane) and independent of the sham/exposure condition, is the snapshot of a sedimentation-independent phenomenon, along the time of the experiments. Furthermore, these results reinforce that the proposed explanation for that differences observed in the movement of

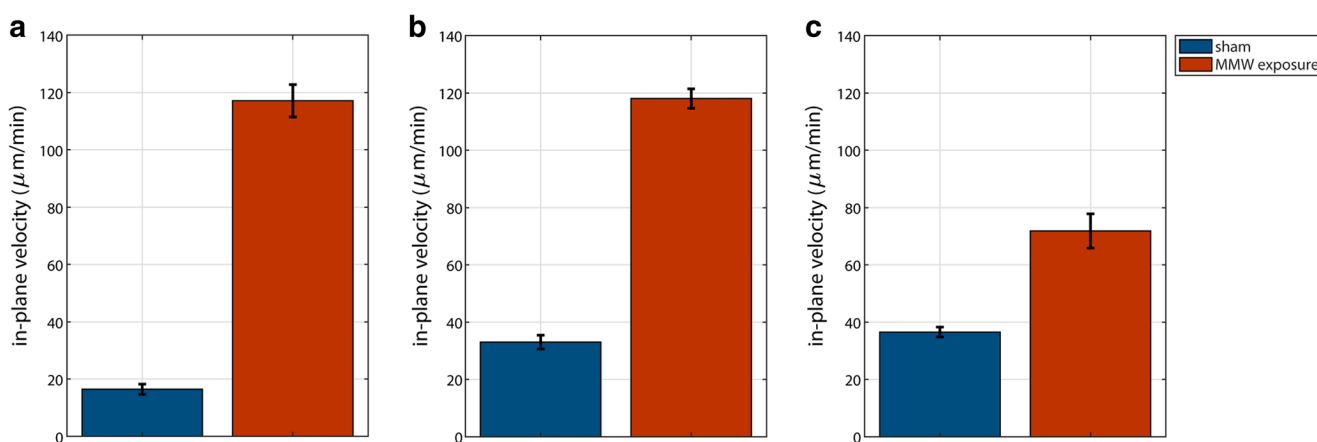


**Fig. 7** Vesicle velocity; average in-plane velocity magnitude (expressed as  $\mu\text{m}/\text{min}$ ) is reported for **a** neutral giant vesicles electroformed, **b** empty GUVs, and **c** MNP-GUVs

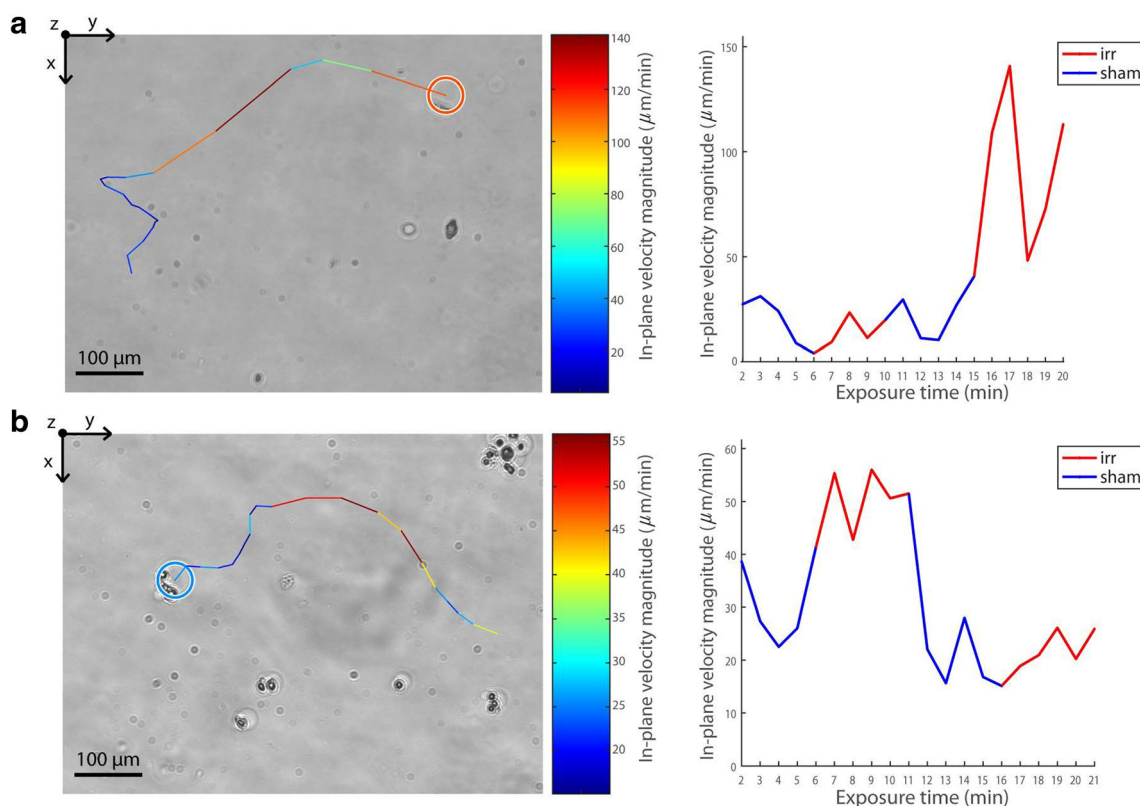


**Fig. 8** Color-coded in-plane velocity (expressed as  $\mu\text{m}/\text{min}$ ) of empty GUVs (a) and MNP-GUVs (b) is shown

vesicles could be in the different distribution of the charge (1) internal to the vesicle membrane and (2) between the internal and external of the membrane, which does influence the action of MMW [10].

In preliminary experiments, we tried to use low concentration of sugar solutions to reduce the possible impact that the viscosity could have on the motion of vesicles without success. The vesicle motion was too fast, and they moved away from the microscope's field of view in a short time making it difficult to perform the observation during sham and irradiation treatments on the same sample, a prerequisite of our study. This observation provides a useful hint for predicting what would be the behavior of vesicles in viscous biological fluids. We predict that a slowdown of the vesicle response should occur due to inertial effects. However, a proper tuning of irradiation conditions could easily allow the control of inertial/deformation effects also in biological fluids such as blood.

### Temperature measurements

To evaluate any possible heating effects of MMW exposure on the specimen, we carefully measured temperature changes and temperature rise rates in the aqueous solution containing either MNP-GUVs or empty GUVs in the observation dish following the indication in literature [52]. A representative example of temperature dynamics recorded during exposure

experiments of MNP-GUVs is shown in Fig. 9. The average temperature increase achieved after 20 min of interrupted regime of exposure (MMW 5 min off then 5 min on) was  $0.15 \pm 0.05$  °C. The same increment was also observed for empty GUVs (data not shown), indicating that though heat generation can be localized within the volume of MNPs [53], under our conditions, negligible temperature increment over the entire volume of the specimen was observed. As a consequence, this small temperature increase could be ascribed to the unavoidable specific absorption rate difference between the boundaries and the bulk, which originates as a consequence of the low penetration depth of MMW. Indeed, in liquid media, most of the incident MMW energy is absorbed within the first few one-tenths of a millimeter [54], and temperature gradients close to the irradiated surface can be high enough to produce different types of convection processes. However, such a temperature increase is considered in the literature to be below the threshold at which its effects should be considered thermally driven [55, 56]. No further temperature increment was observed when the microscope light was switched on for the short time necessary to acquire the images (data not shown).

To achieve a quantitative understanding of the induced change of movement direction in the presence of MMW, the specific absorption rate (SAR) was quantified and correlated with the observed phenomenon. Numerical evaluation of

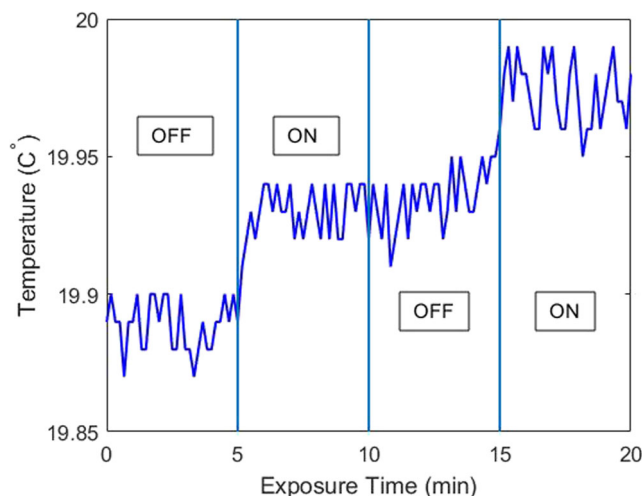


**Fig. 9** Temperature dynamics recorded in a MNP-GUV sample subjected to a time-interrupted exposure regime is shown. The probe tip of thermocouple was positioned in the aqueous solution in the central region of the observation dish, where microscope images were always collected. The time at which the MMW was switch on and off is marked

SAR, extensively described elsewhere [25], indicated that a very uniform distribution of SAR was present in the central region of the dish, covering an area of about  $0.1 \text{ mm}^2$ , where microscope images of dispersed vesicles were always acquired. An average SAR value of  $0.2 \text{ W/kg}$  was calculated in the central region of the dish (see Supplemental Information in Fig. SI-3); this value is significantly smaller than the recommended SAR threshold value below which there is no significant temperature elevation that would affect biosystems ( $0.2$  vs.  $1.6 \text{ W/kg}$ ) [57]. Notably, a negligible elevation of temperature is expected from this SAR level. In fact, in the worst case of no thermal conductivity or convective exchanges, an increase of  $0.014 \text{ }^\circ\text{C}$  of temperature during the 5 min of exposure is expected, i.e., so low that it could not cause local heating of the sample.

Finally, the magnetic response of MNPs can be neglected in the evaluation of the SAR due to the low quantity of MNPs inside the MNP-GUVs and the high exposure frequency applied [58].

## Conclusion

In conclusion, this study described an experimental setup to follow the dynamics of lipid vesicles, in general, and with combinations of magneto nanoparticles when eliciting their response to external stimuli to move directionally. Our results revealed that the membrane composition (neutral vs. charged phospholipids) of giant vesicles modulates the effect induced by MMW exposure on the collective reorientation in vesicle's movement. This knowledge could be used in designing liposomal formulation for improving the effectiveness, for example, of local distribution of liposomal agents.

Furthermore, this study indicates that also negatively charged lipid vesicles containing magnetic nanoparticles, although with MMW-induced response delayed in comparison with negatively charged lipid vesicles alone, change the direction of their motion. For example, it is imagined that using the experimental equivalent to that shown here, it could be possible, in conjunction with magnetic fields, to precisely control the dynamics of vesicles.

The use of millimeter wave opens up new possibilities for characterization and processing of not only liposome vesicle but also other soft matter multiphase systems such as polymer vesicles or biological cells.

Note, that the results were attributed solely to non-thermal phenomena, thus suggesting subtle specific effects not depending on the thermal energy deposited by the MMW on the specimen.

Although, the tests were on micrometer-sized vesicles, which could have a limited value for in vivo applications, new information for future development of electromagnetic field guidance of lipid vesicles to tissue targets has been provided.

## Compliance with ethical standards

**Conflict of interest** The authors declare that they have no conflict of interest.

## References

1. Woodle MC, Newman MS, Cohen JA. Sterically stabilized liposomes: physical and biological properties. *J Drug Target*. 1994;2(5): 397–403. <https://doi.org/10.3109/10611869408996815>.
2. Allen TM, Cullis PR. Drug delivery systems: entering the mainstream. *Science*. 2004;303(5665):1818–22. <https://doi.org/10.1126/science.1095833>.
3. Torchilin VP. Recent advances with liposomes as pharmaceutical carriers. *Nat Rev Drug Discov*. 2005;4(2):145–60. <https://doi.org/10.1038/nrd1632>.
4. Kagan D, Laocharoensuk R, Zimmerman M, Clawson C, Balasubramanian S, Kong D, et al. Rapid delivery of drug carriers propelled and navigated by catalytic nanoshuttles. *Small*. 2010;6(23):2741–7. <https://doi.org/10.1002/sml.201001257>.
5. MacDonald M, Spalding G, Dholakia K. Microfluidic sorting in an optical lattice. *Nature*. 2003;426(6965):421–4. <https://doi.org/10.1038/nature02144>.
6. Zhou R, Wang C. Acoustic bubble enhanced pinched flow fractionation for microparticle separation. *J Micromech Microeng*. 2015;25(8):084005. <https://doi.org/10.1088/0960-1317/25/8/084005>.
7. Baylis JR, Chan KY, Kastrup CJ. Halting hemorrhage with self-propelling particles and local drug delivery. *Thromb Res*. 2016;141(Suppl 2):S36–9.
8. Tabatabaei SN, Duchemin S, Girouard H, Martel S. Towards MR-navigable nanorobotic carriers for drug delivery into the brain. *IEEE Int Conf Robot Autom*. 2012;14:727–32.
9. Dimova R, Riske KA, Aranda S, Bezlyepkina N, Knorr RL, Lipowsky R. Giant vesicles in electric fields. *Soft Matter*. 2007;3(7):817–27.

10. Dimova R, Bezlyepkina N, Jordö MD, Knorr RL, Riske KA, Staykova M, et al. Vesicles in electric fields: some novel aspects of membrane behavior. *Soft Matter*. 2009;5(17):3201–12. <https://doi.org/10.1039/b901963d>.
11. Kolahdouz EM, Salac D. Dynamics of three-dimensional vesicles in dc electric fields. *Phys Rev E*. 2015;92(1):012302. <https://doi.org/10.1103/PhysRevE.92.012302>.
12. Salipante PF, Vlahovska PM. Vesicle deformation in DC electric pulses. *Soft Matter*. 2014;10:3386–93.
13. Salac D. Vesicles in magnetic fields. *Soft Condensed Matter*. 2016; arXiv:1608.05587v1.
14. Alavi M, Karimi N, Safaei M. Application of various types of liposomes in drug delivery systems. *Adv Pharm Bull*. 2017;7(1): 3–9. <https://doi.org/10.15171/apb.2017.002>.
15. Bulbake U, Doppalapudi S, Kommineni N, Khan W. Liposomal formulations in clinical use: an updated review. *Pharmaceutics*. 2017;9(2) <https://doi.org/10.3390/pharmaceutics9020012>.
16. Dai M, Wu C, Fang HM, Li L, Yan JB, Zeng DL, et al. Thermo-responsive magnetic liposomes for hyperthermia-triggered local drug delivery. *J Microencapsul*. 2017;34(4):408–15. <https://doi.org/10.1080/02652048.2017.1339738>.
17. Jain A, Tiwari A, Verma A, Jain SK. Ultrasound-based triggered drug delivery to tumors. *Drug Deliv Transl Res*. 2018;8(1):150–64. <https://doi.org/10.1007/s13346-017-0448-6>.
18. Nappini S, Al Kayal T, Berti D, Nord Èn B, Baglioni P. Magnetically triggered release from giant unilamellar vesicles: visualization by means of confocal microscopy. *J Phys Chem Lett*. 2011;2(7):713–8. <https://doi.org/10.1021/jz2000936>.
19. Ramundo-Orlando A, Longo G, Cappelli M, Girasole M, Tarricone L, Beneduci A, et al. The response of giant phospholipid vesicles to millimeter waves radiation. *Biochim Biophys Acta*. 2009;1788(7): 1497–507. <https://doi.org/10.1016/j.bbamem.2009.04.006>.
20. Rojavin MA, Ziskin MC. Medical application of millimetre waves. *QJM*. 1998;91(1):57–66.
21. Usichenko TI, Edinger H, Gizhko VV, Lehmann C, Wendt M, Feyerherd F. Low-intensity electromagnetic millimeter waves for pain therapy. Evidence-based complementary and alternative medicine. *eCAM*. 2006;3(2):201–7. <https://doi.org/10.1093/ecam/nel012>.
22. Partyla T, Hacker H, Edinger H, Leutzow B, Lange J, Usichenko T. Remote effects of electromagnetic millimeter waves on experimentally induced cold pain: a double-blinded crossover investigation in healthy volunteers. *Anesth Analg*. 2017;124(3):980–5. <https://doi.org/10.1213/ANE.0000000000001657>.
23. Vecchia P, Matthes R, Ziegelberger G, Lin J, Saunders R, Swerdlow A. Exposure to high frequency electromagnetic fields, biological effects and health consequences (100 kHz–300 GHz). *International Commission on Non-Ionizing Radiation Protection*; 2009.
24. Ramundo-Orlando A. Effects of millimeter waves radiation on cell membrane—a brief review. *J Infrared Millimeter Terahertz Waves*. 2010;31(12):1400–11. <https://doi.org/10.1007/s10762-010-9731-z>.
25. Albin M, Dinarelli S, Pennella F, Romeo S, Zampetti E, Girasole M, et al. Induced movements of giant vesicles by millimeter wave radiation. *Biochim Biophys Acta*. 2014;1838(7):1710–8. <https://doi.org/10.1016/j.bbamem.2014.03.021>.
26. Angelakeris M. Magnetic nanoparticles: a multifunctional vehicle for modern therapeutics. *Biochim Biophys Acta*. 2017;1861(6): 1642–51. <https://doi.org/10.1016/j.bbagen.2017.02.022>.
27. Estelrich J, Escribano E, Queralt J, Busquets MA. Iron oxide nanoparticles for magnetically-guided and magnetically-responsive drug delivery. *Int J Mol Sci*. 2015;16(4):8070–101. <https://doi.org/10.3390/ijms16048070>.
28. Shirmardi Shaghasemi B, Virk MM, Reimhult E. Optimization of magneto-thermally controlled release kinetics by tuning of magnetoliposome composition and structure. *Sci Rep*. 2017;7(1): 7474. <https://doi.org/10.1038/s41598-017-06980-9>.
29. Preiss MR, Bothun GD. Stimuli-responsive liposome-nanoparticle assemblies. *Expert Opin Drug Deliv*. 2011;8(8):1025–40. <https://doi.org/10.1517/17425247.2011.584868>.
30. Kuster N, Schonborn F. Recommended minimal requirements and development guidelines for exposure setups of bio-experiments addressing the health risk concern of wireless communications. *Bioelectromagnetics*. 2000;21(7):508–14.
31. Pautot S, Frisken BJ, Weitz DA. Production of unilamellar vesicles using an inverted emulsion. *Langmuir*. 2003;19(7):2870–9. <https://doi.org/10.1021/la026100v>.
32. Carrara P, Stano P, Luisi PL. Giant vesicles “colonies”: a model for primitive cell communities. *ChemBiochem*. 2012;13(10):1497–502. <https://doi.org/10.1002/cbic.201200133>.
33. Saywell LG, Cunningham BB. Determination of Iron: colorimetric o-phenanthroline method. *Ind Eng Chem Anal Ed*. 1937;9(2):67–9. <https://doi.org/10.1021/ac50106a005>.
34. Zhao JX. Numerical dosimetry for cells under millimetre-wave irradiation using Petri dish exposure set-ups. *Phys Med Biol*. 2005;50(14): 3405–21. <https://doi.org/10.1088/0031-9155/50/14/015>.
35. Mally M, Majhenc J, Svetina S, Zeks B. The response of giant phospholipid vesicles to pore-forming peptide melittin. *Biochim Biophys Acta*. 2007;1768(5):1179–89. <https://doi.org/10.1016/j.bbamem.2007.02.015>.
36. Riske KA, Dimova R. Electro-deformation and poration of giant vesicles viewed with high temporal resolution. *Biophys J*. 2005;88(2):1143–55. <https://doi.org/10.1529/biophysj.104.050310>.
37. Hough PVC. Method and means for recognizing complex pattern. US Patent No3069654. 1962.
38. Chiba M, Miyazaki M, Ishiwata S. Quantitative analysis of the lamellarity of giant liposomes prepared by the inverted emulsion method. *Biophys J*. 2014;107(2):346–54. <https://doi.org/10.1016/j.bpj.2014.05.039>.
39. Bonnaud C, Monnier CA, Demurtas D, Jud C, Vanhecke D, Montet X, et al. Insertion of nanoparticle clusters into vesicle bilayers. *ACS Nano*. 2014;8(4):3451–60. <https://doi.org/10.1021/nn406349z>.
40. Giardini PA, Fletcher DA, Theriot JA. Compression forces generated by actin comet tails on lipid vesicles. *Proc Natl Acad Sci U S A*. 2003;100(11):6493–8. <https://doi.org/10.1073/pnas.1031670100>.
41. Husen P, Fidorra M, Hartel S, Bagatolli LA, Ipsen JH. A method for analysis of lipid vesicle domain structure from confocal image data. *Eur Biophys J*. 2012;41(2):161–75. <https://doi.org/10.1007/s00249-011-0768-2>.
42. Rey Suarez I, Leidy C, Tellez G, Gay G, Gonzalez-Mancera A. Slow sedimentation and deformability of charged lipid vesicles. *PLoS One*. 2013;8(7):e68309. <https://doi.org/10.1371/journal.pone.0068309>.
43. Pasenkiewicz-Gierula M, Baczynski K, Markiewicz M, Murzyn K. Computer modelling studies of the bilayer/water interface. *Biochim Biophys Acta*. 2016;1858(10):2305–21. <https://doi.org/10.1016/j.bbamem.2016.01.024>.
44. Chukova YP. Doubts about nonthermal effects of MM radiation have no scientific foundations. *J Phys Conf Ser*. 2011;329(1) <https://doi.org/10.1088/1742-6596/329/1/012032>.
45. Beneduci A, Bernstein E. Review on the mechanisms of interaction between millimeter waves and biological systems. *Bioelectrochem Res Dev*. 2008:35–80.
46. Chukova YP. Reasons of poor replicability of nonthermal bioeffects by millimeter waves. *Bioelectrochem Bioenerg*. 1999;48(2):349–53.
47. Vlahovska PM, Gracia RS, Aranda-Espinoza S, Dimova R. Electrohydrodynamic model of vesicle deformation in alternating electric fields. *Biophys J*. 2009;96(12):4789–803. <https://doi.org/10.1016/j.bpj.2009.03.054>.
48. Seiwert J, Vlahovska PM. Instability of a fluctuating membrane driven by an ac electric field. *Phys Rev E Stat Nonlinear Soft*



- Matter Phys. 2013;87(2):022713. <https://doi.org/10.1103/PhysRevE.87.022713>.
49. Monnier CA, Burnand D, Rothen-Rutishauser B, Lattuada M, Petri-Fink A. Magnetoliposomes: opportunities and challenges. *Eur J Nanomed*. 2014;6(4):201–15. <https://doi.org/10.1515/ejnm-2014-0042>.
  50. Schulz M, Olubummo A, Binder WH. Beyond the lipid-bilayer: interaction of polymers and nanoparticles with membranes. *Soft Matter*. 2012;8(18):4849–64. <https://doi.org/10.1039/c2sm06999g>.
  51. Man D, Olchawa R. Dynamics of surface of lipid membranes: theoretical considerations and the ESR experiment. *Eur Biophys J*. 2017;46(4):325–34. <https://doi.org/10.1007/s00249-016-1172-8>.
  52. Darros-Barbosa R, Balaban MO, Teixeira AA. Temperature and concentration dependence of heat capacity of model aqueous solutions. *Int J Food Prop*. 2003;6(2):239–58. <https://doi.org/10.1081/JFP-120017845>.
  53. Koblinski P, Cahill DG, Bodapati A, Sullivan CR, Taton TA. Limits of localized heating by electromagnetically excited nanoparticles. *J Appl Phys*. 2006;100(5) <https://doi.org/10.1063/1.2335783>.
  54. Khizhnyak EP, Ziskin MC. Temperature oscillations in liquid media caused by continuous (nonmodulated) millimeter wavelength electromagnetic irradiation. *Bioelectromagnetics*. 1996;17(3):223–9. [https://doi.org/10.1002/\(SICI\)1521-186X\(1996\)17:3<223::AID-BEM8>3.0.CO;2-5](https://doi.org/10.1002/(SICI)1521-186X(1996)17:3<223::AID-BEM8>3.0.CO;2-5).
  55. Schuderer J, Samaras T, Oesch W, Spät D, Kuster N. High peak SAR exposure unit with tight exposure and environmental control for in vitro experiments at 1800 MHz. *IEEE Trans Microwave Theory Tech*. 2004;52(8 II):2057–66. <https://doi.org/10.1109/TMTT.2004.832009>.
  56. Zhao J. In vitro dosimetry and temperature evaluations of a typical millimeter-wave aperture-field exposure setup. *IEEE Trans Microwave Theory Tech*. 2012;60(11):3608–22. <https://doi.org/10.1109/TMTT.2012.2213829>.
  57. IEEE standard for safety levels with respect to human exposure to radio frequency electromagnetic fields, 3 kHz to 300 GHz. *IEEE Standard for Safety Levels with Respect to Human Exposure to Radio Frequency Electromagnetic Fields, 3 KHz to 300 GHz*. 1992.
  58. Fannin P, Relihan T, Charles S. Experimental and theoretical profiles of the frequency-dependent complex susceptibility of systems containing nanometer-sized magnetic particles. *Phys Rev B Condens Matter Mater Phys*. 1997;55(21):14423–8. <https://doi.org/10.1103/PhysRevB.55.14423>.